



Plasmonic effects of silver nanoparticles with various dimensions embedded and non-embedded in silicon dioxide antireflective coating on silicon solar cells

Wen-Jeng Ho¹ · Sheng-Kai Fen¹ · Jheng-Jie Liu¹

Received: 15 July 2017 / Accepted: 5 December 2017 / Published online: 7 December 2017
© Springer-Verlag GmbH Germany, part of Springer Nature 2017

Abstract

Plasmonic effects of silver nanoparticles (Ag NPs) of various dimensions embedded and non-embedded in silicon dioxide antireflective coating (SiO₂ ARC) deposited by electron-beam evaporation on silicon (Si) solar cells are characterized. Raman scattering and absorbance measurements were used to examine plasmonic resonance absorption of Ag NPs with various particle dimensions and different dielectric environments. The obtained Raman and absorbance results revealed that the large dimensions of Ag NPs exhibited much impressive plasmonic resonance absorption. Furthermore, optical reflectance and photovoltaic current–voltage measurements were also used to confirm the photovoltaic performance enhancement inducing by plasmonic forward scattering of Ag NPs of various dimensions. Thus, the efficiency enhancement of 3.64, 7.42, and 10.24% for the solar cells with Ag NPs in diameter of 21, 25, 32 nm, respectively, embedded in SiO₂ ARC was achieved due to plasmonic scattering inducing by Ag NPs, compared to the cell with a pure SiO₂ ARC without Ag NPs.

1 Introduction

A surface plasmon resonance (SPR) is the resonance oscillation of collective conduction electrons in a metal stimulated by beam of light incident. The resonance condition is established when the frequency of light matches the natural frequency of conduction electrons oscillating against from this restoring force. SPR in nanometer-sized structures is called localized surface plasmon resonance (LSPR). LSPRs are non-propagating excitations of the conduction electrons of metallic NPs coupled to the electromagnetic field and the collective conduction electrons oscillation causes a large resonant enhancement of the local field near the NP [1–5]. For gold (Au) and silver (Ag) nanoparticles (NPs), the resonance falls into the visible region of the electromagnetic spectrum. Thus, the LSPR properties of Au NPs and Ag NPs have attracted attention for applications on optical devices because of the significant enhancement and confinement of the electric fields near metallic nanoparticle/dielectric

interfaces [6, 7]. Typically, Ag NPs are extraordinarily efficient at absorbing and scattering light. The strong interaction of the Ag NPs with light occurs because the conduction electrons on the silver surface undergo a collective oscillation when excited by light at specific wavelengths [8, 9]. This oscillation results in unusually strong light scattering and absorption properties. In addition, the SPR of metallic NPs is sensitive to the particle size, shape, dielectric properties of the metal and the surrounding medium [10–15]. A unique property of spherical Ag NPs is that this SPR peak wavelength can be tuned from 400 to 530 nm by changing the particle size and the local refractive index near the particle surface. Even larger shifts of the SPR peak wavelength out into the infrared region of the electromagnetic spectrum can be achieved by producing Ag NPs with rod or plate shapes [9, 16, 17]. Tuning of the LSPR spectrum associated with metallic NPs closely match the solar spectrum, which increasing the optical absorption of incident photons within the active layer as well as increasing the photocurrent of device, is an important issues [6, 8, 18–27]. However, to our knowledge, only limited study has been conducted on plasmonic effects of Ag NPs of various dimensions embedded and non-embedded in silicon dioxide antireflective coating (SiO₂ ARC) on silicon solar cells [15, 28]

In the present study, surface plasmon resonances of Ag NPs with various particle-dimensions and different

✉ Wen-Jeng Ho
wjho@ntut.edu.tw

¹ Department of Electro-Optical Engineering, National Taipei University of Technology, No. 1, Sec. 3, Zhongxial E. Rd., Taipei 10608, Taiwan, ROC

dielectric-environments were first examined using Raman scattering and absorbance measurements [29, 30]. In addition, optical reflectance, internal quantum efficiency (IQE), and photovoltaic current density–voltage (J – V) of the cells with Ag NPs of various dimensions embedded and non-embedded in SiO_2 ARC on silicon solar cells were measured and compared. Through comparisons with reference cells, the photovoltaic performance enhancements of the cells with Ag NPs of various dimensions deposited on a thin SiO_2 layer or embedded in SiO_2 ARC are confirmed due to the plasmonic forward scattering inducing by Ag NPs.

2 Experimental details

Nano-scale metallic particles with surface plasmons can be used to enhance Raman scattering and manipulate the light for photovoltaic devices to enhance its efficiency. In this study, the excitation of localized surface plasmon of the proposed Ag NPs with various dimension embedded and non-embedded in SiO_2 layer was examined by surface enhanced Raman scattering and absorbance measurements. Next, the plasmonics light scattering modulation of various Ag NPs embedded and non-embedded in SiO_2 ARC on the Si solar cells was also characterization using optical reflectance and J – V measurements.

2.1 Raman scattering and absorbance produced by metallic nanoparticles

To characterize the plasmon-enhanced Raman scattering and absorbance produced by metallic nanoparticles, the samples were prepared as: (1) samples of Ag NPs non-embedded in SiO_2 layer: 3-, 5-, and 7-nm thick Ag films were, respectively, deposited on the glass substrates with a 20 nm-thick layer of SiO_2 using E-beam evaporation. The samples were then annealed at 200 °C for 30 min under ambient H_2 to form Ag NPs (Fig. 1a); (2) Samples of Ag NPs embedded in SiO_2 layer: 3-, 5-, and 7-nm thick Ag films were first deposited, respectively, on the glass substrates with a 20 nm-thick

layer of SiO_2 using E-beam evaporation. The samples were then annealed at 200 °C for 30 min under ambient H_2 to form Ag NPs. Next, a 74-nm thick SiO_2 film was deposited over the surface of Ag NPs using E-beam evaporation (Fig. 1b); (3) We also deposited a 94 nm thick SiO_2 layer on the glass substrate without metallic NPs as a reference sample for comparison (Fig. 1c). Raman scattering spectra were collected using a micro-Raman system (Ramboss 500i Micro-Raman/PL Spectroscopy, DONGWOO) with a semiconductor laser operating at 473 nm and with an output power of 0.09 mW as the excitation source. Besides, absorbance spectra were collected using a miniature spectrometer (USB4000, Ocean Optics) with a deuterium tungsten light source (200–2000 nm) and a 5 cm diameter reflective integrating sphere.

2.2 Fabrication of plasmonic silicon solar cells

P-type crystalline silicon wafers with a (100) orientation and resistivity of 10 Ω -cm with a thickness of 525 μm were used as a base material for solar cell devices after being cut to samples of 1 \times 1 cm^2 . Following RCA standard-cleaning processes, the silicon samples were coated with a phosphorus liquid source (Phosphorofilm, Emulsitone Co., New Jersey, US) using spin-on coating at a speed of 3000 rpm for 20 s. They were then prebaked at 200 °C for 5 min followed by further baking at 400 °C for 10 min in a rapid thermal annealing (RTA) chamber for the removal of organic species. The front and back sides of the samples were then capped using a layer of SiO_2 (300-nm thick) using e-beam evaporation before being heated in an RTA chamber at 925 °C under ambient N_2 with 1–2% O_2 for 90 s to initiate the diffusion of phosphorus and thereby obtain an n^+ -Si emitter layer (n^+ -Si emitter/p-Si base). The samples were then soaked in a solution of hydrofluoric acid to remove the layers of SiO_2 and phosphosilicate glass before undergoing isolation etching using a photolithographic process using a solution of HNO_3 : HF : H_2O at a ratio of 1:1:2, which resulted in individual cells 4 \times 4 mm^2 in size. Ohmic contact electrodes were produced by depositing a layer of aluminum (Al) film

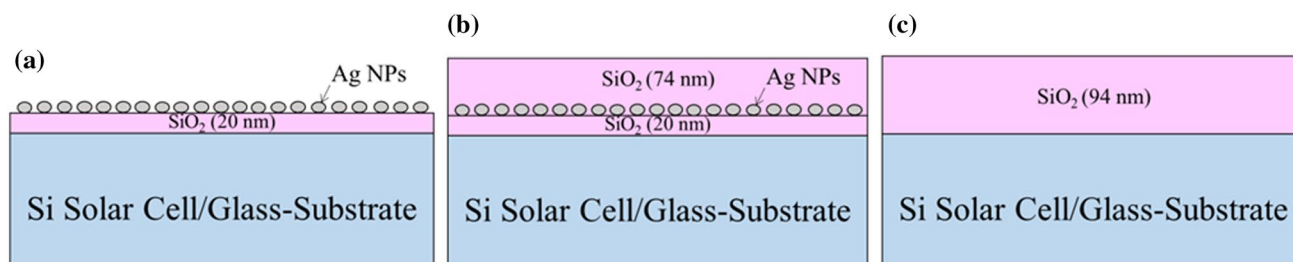


Fig. 1 **a** Ag NPs on a thin SiO_2 layer, **b** Ag NPs embedded in SiO_2 ARC layer, **c** a pure SiO_2 ARC layer. All proposed schemes were coated on the glass substrates and Si solar cells, respectively

to a thickness of 300 nm on the back side and Ti (20-nm)/Al (300-nm) films on the front side using e-beam evaporation. The final step in the fabrication of the bare Si solar cells involved annealing under ambient N_2 at 450 °C for 10 min to ensure a good ohmic contact between the metallic electrodes and Si semiconductor.

Plasmonic Si solar cells were fabricated by depositing a 20-nm thick SiO_2 spacer layer on the top surface of the bare solar cells using e-beam evaporation. The SiO_2 film was evaporated under pressure of 1.50×10^{-4} Pa with an emission current of 22 mA, which resulted in a deposition rate of 0.32 Å/s. As shown in Fig. 1, a variety of Si solar cell samples were produced from the bare substrate to investigate the light scattering of Ag NPs of various particle dimension schemes: the cell with Ag NPs non-embedded in SiO_2 layer (Fig. 1a), the cell with Ag NPs embedded in SiO_2 ARC (Fig. 1b), and the cell with a pure SiO_2 ARC without Ag NPs (Fig. 1c). The morphology and dimensions of the Ag NPs were characterized using electron scanning microscopy (SEM; JEOL JSM-6500F) and the size distribution of the particles was calculated from SEM images using J-image software (National Institute of Mental Health, Bethesda, MD, USA). We then characterized the optical and electrical performance of the resulting plasmonic Si solar cells based on the measurements of optical reflectance (Lambda 35, PerkinElmer, Inc., Waltham, Massachusetts, USA), IQE response at wavelengths between 300 and 1000 nm (Enli Technology Co., Ltd.), and photovoltaic J–V under AM 1.5G (1000 mW/cm² at 25 °C) solar simulation. The solar simulator (XES-151S, San-Ei Electric Co., Ltd.) was calibrated using a crystalline silicon reference cell (PVM-236) certified by the National Renewable Energy Laboratory (NREL) prior to measurements.

3 Results and discussion

Figure 2 shows SEM images of Ag NPs and the size distribution and surface coverage of Ag NPs, as calculated using ImageJ software from the corresponding SEM images deposited as an Ag film to thicknesses of (a) 3 nm, (b) 5 nm and (c) 7 nm, respectively. Because the plasmonic light scattering induced by Ag-NPs was depended on the samples with Ag NPs of various size distribution profiles. The average surface coverage and average diameter of the obtained Ag NPs were as follows: 36.75% and 20.13 nm, 41.83% and 25.03 nm, and 46.46% and 32.14 nm, corresponding to the deposited Ag film to thicknesses of (a) 3 nm, (b) 5 nm and (c) 7 nm. Thus, the surface coverage and diameter of Ag NPs increase when the deposited Ag film thickness increased.

The most intense surface-enhanced Raman scattering (SERS) signals are obtained from Ag NPs of various size and shape. Figure 3 shows the Raman spectra of samples

with the following configurations, Fig. 3a: 20-nm SiO_2 , Ag-NPs (3 nm)/ SiO_2 , Ag NPs (5 nm)/ SiO_2 , and Ag NPs (7 nm)/ SiO_2 ; Fig. 3b: 94-nm SiO_2 , Ag NPs (3 nm) embedded in SiO_2 , Ag NPs (5 nm) embedded in SiO_2 , and Ag NPs (7 nm) embedded in SiO_2 . Typically, the intensity of the Raman signals was enhanced by surface plasmon resonance of the metallic NPs, compared to that of the sample comprising only an SiO_2 on the glass substrate and a higher Raman signal intensity was exhibited on the sample with the large dimensions and high coverage of Ag NPs. The samples of Ag NPs non-embedded in SiO_2 ARC presented five Raman signal intensity peaks (plasmon resonance modes) at 861, 1144, 1294, 1415, and 1625 cm⁻¹ and the samples of Ag NPs embedded in SiO_2 ARC also presented five Raman signal intensity peaks at 860, 1142, 1372, 1408, and 1624 cm⁻¹. However, the peak at 1294 cm⁻¹ mode was suppressed and the 1415 cm⁻¹ mode was split into 1372 and 1408 cm⁻¹ modes because the refractive index (*n*) of the up-side surface of the Ag NPs is increased [from *n* = 1 (air) to *n* = 1.5 (SiO_2)] when Ag NPs embedded in SiO_2 layer. Furthermore, the Raman peaks can be assigned to the molecular vibrations in Ag/ SiO_2 composites as follows [31, 32]: (1) the 861 cm⁻¹ Raman band was the ring stretching of Ag-O-Ag; (2) the 1144 cm⁻¹ Raman band was the asymmetric stretching of Si-O-Si; (3) the 1294 cm⁻¹ Raman band was the bending of Si-O-Si; (4) the 1372 cm⁻¹ Raman band was the stretching of Ag[O-O]⁻, and (5) the 1625 cm⁻¹ Raman band was the overtone of Ag-OH. In conclusion, we observed a strong local electric field associated with the surface plasmon resonance of Ag NPs in this study.

Ag NPs absorb and scatter light with extraordinary efficiency. Their strong interaction with light occurs because the conduction electrons on the metal surface undergo a collective oscillation when they are excited by light at specific wavelengths. Ag NPs absorption and scattering properties can be tuned by controlling the particle size, shape, and the local refractive index near the particle surface. Figure 4 shows the absorbance spectra of samples with the following configurations, Fig. 4a: 20-nm SiO_2 , Ag-NPs (3 nm)/ SiO_2 , Ag NPs (5 nm)/ SiO_2 , and Ag NPs (7 nm)/ SiO_2 ; Fig. b: 94-nm SiO_2 , Ag NPs (3 nm) embedded in SiO_2 , Ag NPs (5 nm) embedded in SiO_2 , and Ag NPs (7 nm) embedded in SiO_2 . The optical properties of Ag NPs are highly dependent on the nanoparticle diameter. Smaller nanoparticles primarily absorb light and have peaks near 410 nm, while larger particles exhibit increased scattering and have peaks that broaden and shift towards longer wavelength (419 nm), as shown in Fig. 4a. Ag NPs optical properties also depend on the refractive index near the surface of nanoparticle. As the refractive index near the surface of nanoparticle increases, the nanoparticle absorbance peak shifts to longer wavelengths as shown in Fig. 4b, compared to Fig. 4a. Practically, this means

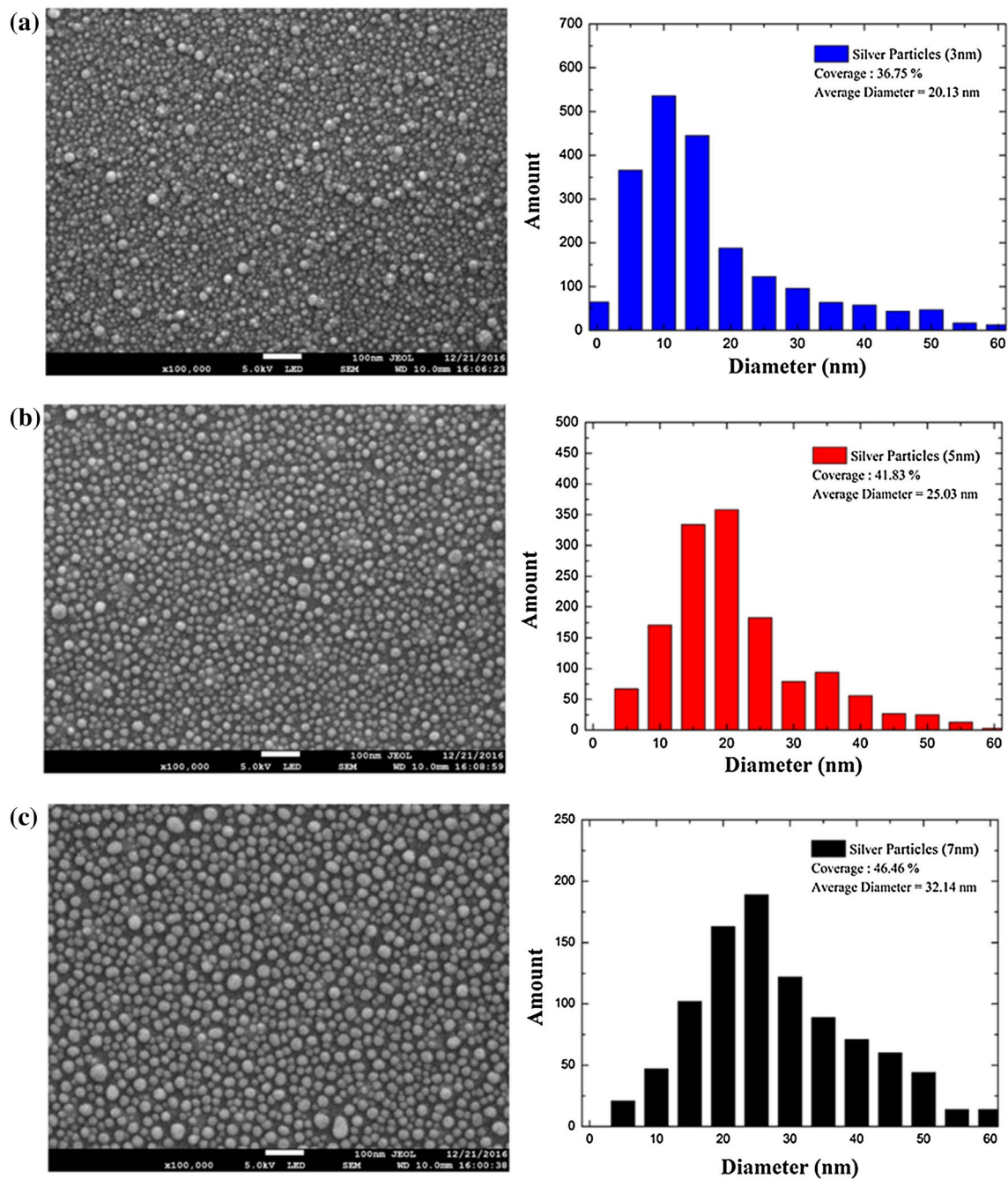


Fig. 2 SEM image and size distribution and surface coverage of Ag-NPs obtained from the deposited Ag film to thicknesses of **a** 3 nm, **b** 5 nm and **c** 7 nm

that the nanoparticle absorbance peak location will shift to longer wavelengths if the Ag NPs embedded in SiO_2 . Thus, in this study, increasing the refractive index (n) of the up-side surface of nanoparticle from $n = 1$ (air) to $n = 1.5$ (SiO_2) results in an absorbance peak shift of over 30 nm. In general, we observed that the surface plasmon resonance band of proposed Ag NPs scheme exhibited at the wavelength range of 350–550 nm in this study.

Figure 5 shows the optical reflectance spectra of the proposed samples. The reflectance of the cells with a thin SiO_2 space layer of 20 nm or with an SiO_2 ARC was lower than that of the bare cell, due to the antireflective properties of the SiO_2 . In Fig. 5a, at wavelengths of 350–550 nm, the reflectance of the cell with Ag NPs of various particle-dimensions on the SiO_2 layer was lower than that of the cell with only an SiO_2 layer, due to the surface plasmon resonance absorption

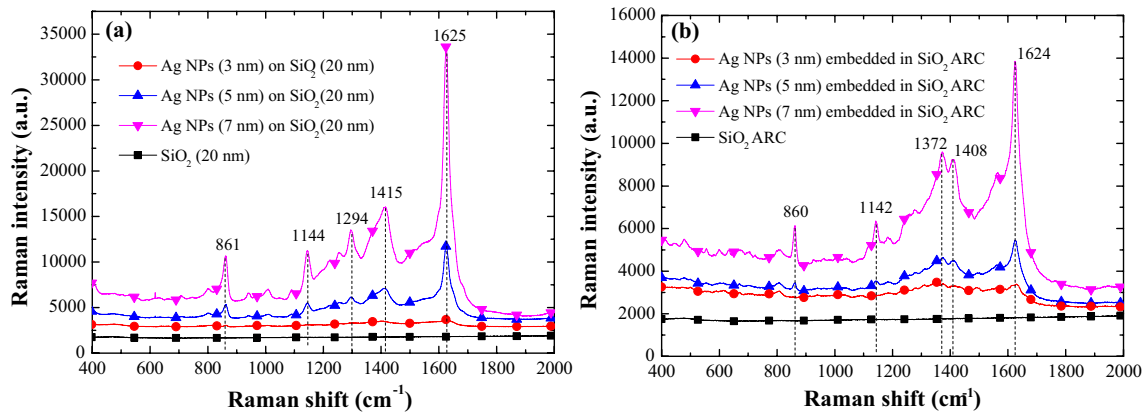


Fig. 3 Raman spectra of samples with the following configurations, **a**: 20-nm SiO₂, Ag-NPs (3 nm)/SiO₂, Ag NPs (5 nm)/SiO₂, and Ag NPs (7 nm)/SiO₂; **b**: 94-nm SiO₂, Ag NPs (3 nm) embedded in SiO₂, Ag NPs (5 nm) embedded in SiO₂, and Ag NPs (7 nm) embedded in SiO₂

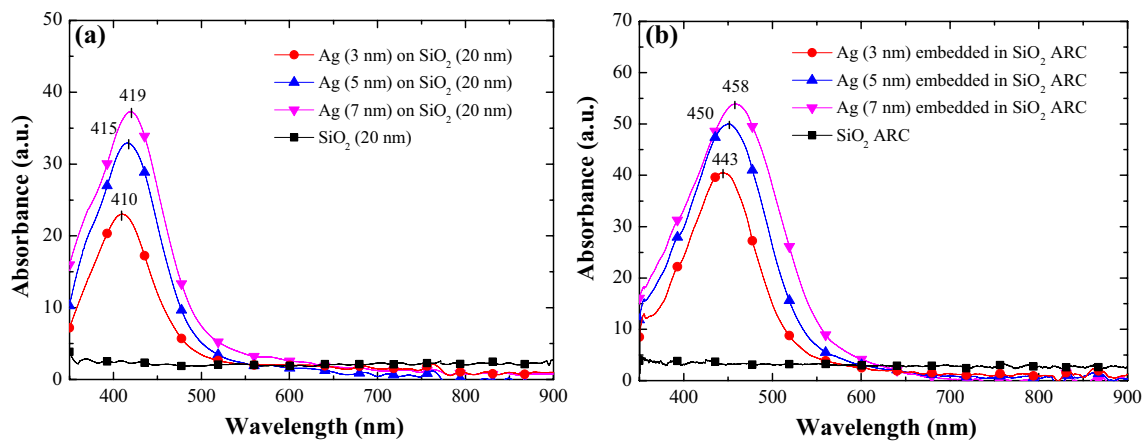


Fig. 4 Absorbance spectra of glass-substrates with the following configurations: **a** 20-nm SiO₂, Ag-NPs (3 nm) on SiO₂ (20 nm), Ag NPs (5 nm) on SiO₂ (20 nm), and Ag NPs (7 nm) on SiO₂ (20 nm); **b**

94-nm SiO₂, Ag NPs (3 nm) embedded in SiO₂ ARC, Ag NPs (5 nm) embedded in SiO₂ ARC, and Ag NPs (7 nm) embedded in SiO₂ ARC

induced by Ag NPs. It should be noted that at wavelengths of 600–1100 nm, the reflectance of the cell with Ag NPs on the SiO₂ layer decreased to a level below that of the cell with only an SiO₂ layer, due to the plasmonic forward scattering of photons induced by the Ag NPs. Furthermore, the reflectance of the cell with large-dimension Ag NPs (7 nm) was lower than that of small-dimension Ag NPs (5 or 3 nm) ones, which agree to the results of Raman and absorbance of high plasmonic effects induced by larger Ag NPs dimensions. Similarly, for Ag NPs embedded in SiO₂ ARC case, the reflectance of the cells with Ag NPs was lower than that the cell with a pure SiO₂ ARC due to the plasmonic effects induced by Ag NPs, as shown in Fig. 5b. Particularly, the reflectance of the cell with Ag NPs embedded in SiO₂ ARC was much lower than the cell with Ag NPs embedded in SiO₂ (non-embedded one) and the reflective trough of the cell with Ag NPs embedded in SiO₂ ARC was red shifted

when the particle dimension was increased. Optical transmittance spectra of the glass-substrates coated with 94-nm SiO₂ ARC, Ag NPs (3 nm) embedded in SiO₂ ARC, Ag NPs (5 nm) embedded in SiO₂ ARC, and Ag NPs (7 nm) embedded in SiO₂ ARC are presented in Fig. 5c for further comparison. In general, a lower reflectance on the photovoltaic devices would be benefited to enhance photocurrent and conversion efficiency.

Internal quantum efficiency (IQE) is the ratio of the number of charge carriers collected by the solar cell to the number of photons of a given energy that shine on the solar cell from outside and are absorbed by the cell. Figure 6 presents the IQE response of the bare silicon solar cell, the cell coated with an SiO₂ ARC layer, and solar cells coated with Ag NPs of various sizes embedded in SiO₂ ARC layer. The IQE responses of the cells with an SiO₂ ARC layer and the cells with Ag NPs embedded in SiO₂ ARC layer are

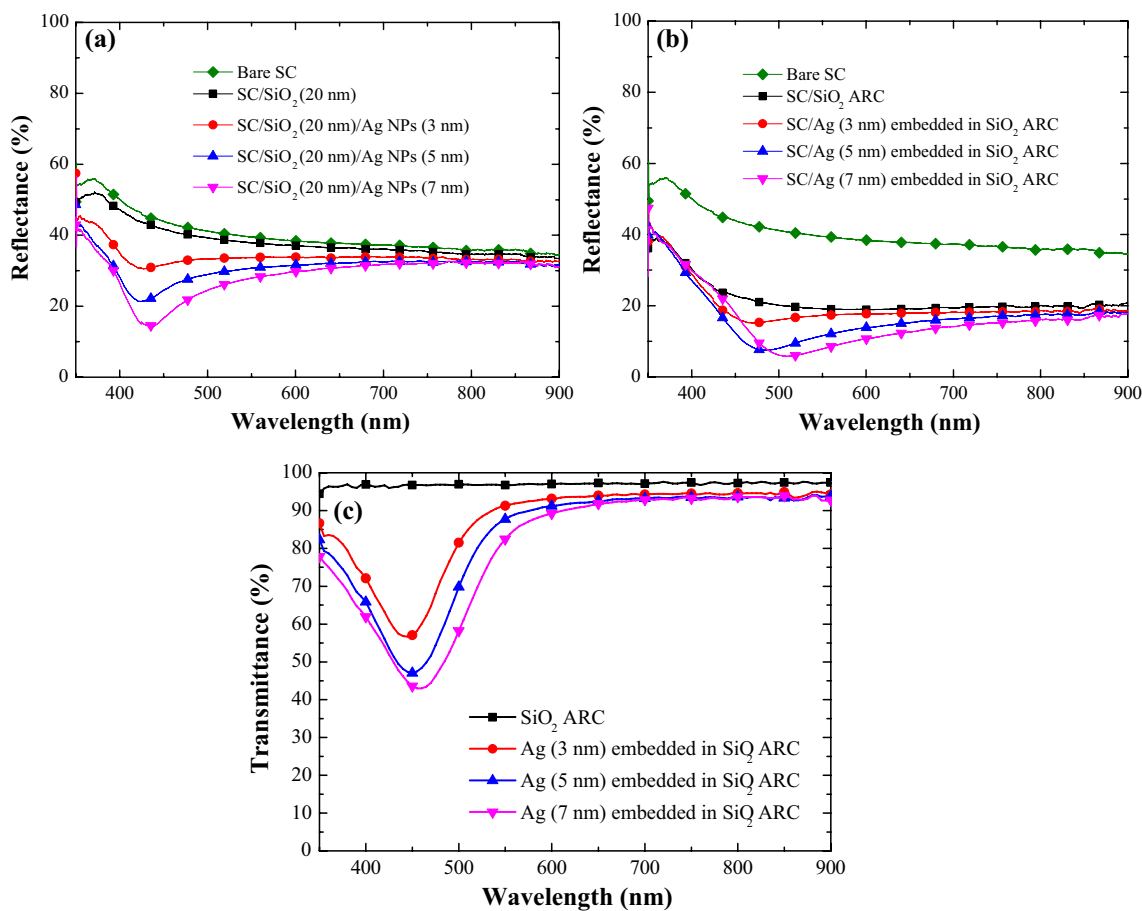


Fig. 5 Optical reflectance spectra showing, **a**: the cells coated with: 20-nm SiO₂, Ag-NPs (3 nm) on SiO₂ (20 nm), Ag NPs (5 nm) on SiO₂ (20 nm), and Ag NPs (7 nm) on SiO₂ (20 nm); **b**: the cells coated with: 94-nm SiO₂ ARC, Ag NPs (3 nm) embedded in SiO₂ ARC, Ag NPs (5 nm) embedded in SiO₂ ARC, and Ag NPs (7 nm)

embedded in SiO₂ ARC. **c** Optical transmittance spectra of the glass-substrates coated with 94-nm SiO₂ ARC, Ag NPs (3 nm) embedded in SiO₂ ARC, Ag NPs (5 nm) embedded in SiO₂ ARC, and Ag NPs (7 nm) embedded in SiO₂ ARC

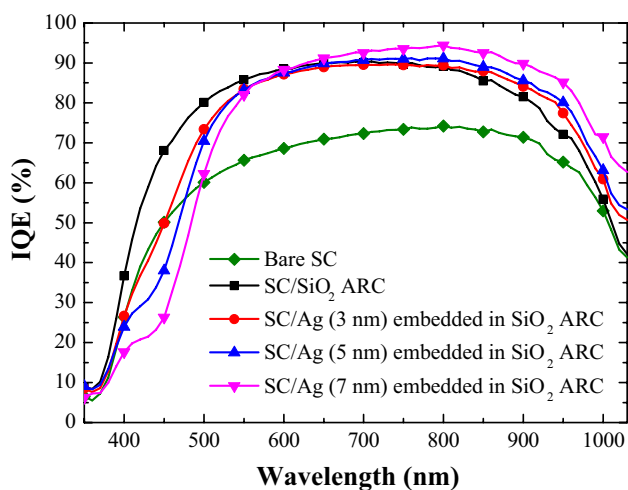


Fig. 6 IQE response of the bare Si solar cell, the cell coated with an SiO₂ ARC layer, and solar cells coated with Ag NPs of various sizes embedded in SiO₂ ARC layer

in strong agreement with the optical reflectivity results. At wavelengths of 350–550 nm, the IQE values of cells with Ag NPs were lower than those of cells with only an SiO₂ layer and the bare cell. This can be attributed to the surface plasmon resonance absorption of Ag NPs. In contrast, at wavelengths of 550–900 nm, the IQE values of cells with Ag NPs were higher than those of cells with only an SiO₂ layer and the bare cell, which are benefited from the plasmonics forward scattering of Ag NPs. The forward scatter photons within the active layer of cells provide far higher collection efficiency, which generates higher photocurrent.

The photovoltaic J–V characteristics of (a) the cells with Ag NPs on a thin SiO₂ space layer and (b) the cells with Ag NPs embedded in SiO₂ ARC are presented in Fig. 7. The photovoltaic performance of all evaluated solar cells is listed in Table 1. In Fig. 7a, the case of the cells with a thin SiO₂ space layer (20 nm), the conversion efficiency (η) enhancement was about 4.55% (from 11.45 to 11.97%) due to antireflection of SiO₂ layer, compared to

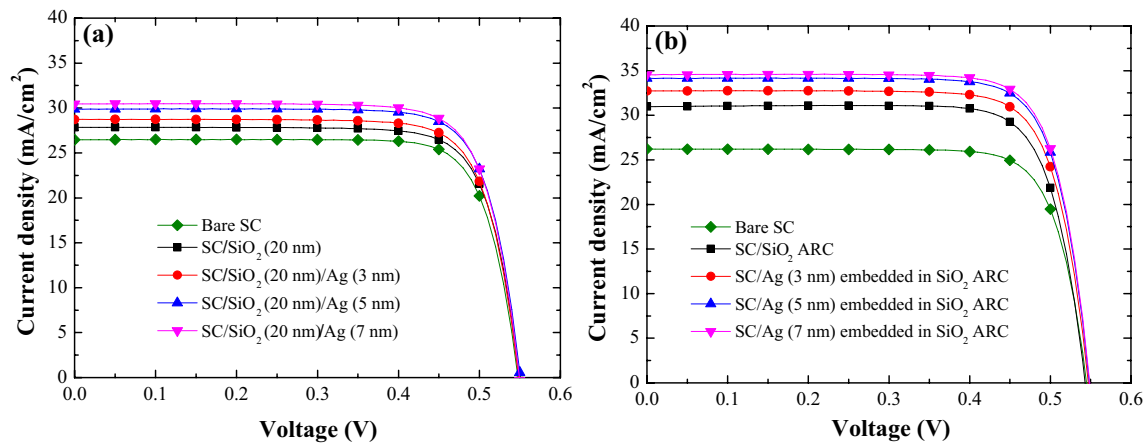


Fig. 7 Photovoltaic current density–voltage (J – V) characteristics, **a**: the cells with Ag NPs on a thin SiO_2 space layer, **b**: the cells with Ag NPs embedded in SiO_2 ARC

Table 1 The photovoltaic performance of all evaluated solar cells

	Cell with Ag NPs on thin SiO_2 layer (20 nm)					Cell with Ag NPs embedded in SiO_2 ARC				
	Bare SC	SiO_2	Ag 3 nm	Ag 5 nm	Ag 7 nm	Bare SC	SiO_2 ARC	Ag 3 nm	Ag 5 nm	Ag 7 nm
V_{oc} (mV)	547.77	549.42	548.6	550.85	549.52	544.32	543.08	547.17	548.47	548.99
J_{sc} (mA/cm^2)	26.48	27.84	28.72	29.87	30.45	26.26	31.67	32.71	34.15	34.54
F.F. (%)	79.06	78.27	78.02	78.27	77.82	78.98	78.37	77.97	78.23	78.32
η (%)	11.45	11.97	12.30	12.88	13.02	11.28	13.47	13.96	14.47	14.85
ΔJ_{sc} (%)	–	5.13	8.46	12.80	14.99	–	20.60	24.56	30.05	31.53
$\Delta \eta$ (%)	–	4.55	7.42	12.49	13.71	–	19.41	23.76	28.28	31.65

the bare cell. For the cells with Ag NPs on a thin SiO_2 space layer, an increasing in short-circuit current–density (J_{sc}) and η is also obtained due to the contribution of plasmonic effects of Ag NPs. Thus, the cells with Ag NPs of dimensions of 21, 25, and 32 nm on thin SiO_2 space layer (non-embedded in SiO_2 scheme), the efficiency enhancement ($\Delta \eta$) of 2.76% (from 11.97 to 12.30%), 7.60% (from 11.97 to 12.88%), and 8.88% (from 11.97 to 13.02%), respectively, were obtained, compared to the cell with a thin SiO_2 space layer without Ag NPs. An increasing significantly in J_{sc} and η was found when the cells coated with a large dimension of Ag NPs. Similarly, in Fig. 7b, the cells with Ag NPs embedded in SiO_2 , J_{sc} and η were (32.71 mA/cm^2 , 13.96%), (34.15 mA/cm^2 , 14.47%), and (34.54 mA/cm^2 , 14.85%) corresponding to Ag NPs of dimensions of 21, 25, and 32 nm, compared to the cell with a pure SiO_2 ARC (31.67 mA/cm^2 , 13.47%). An enhancing further in J_{sc} and η to the cells with Ag NPs embedded in SiO_2 ARC was attributed to the combination of the plasmonic effects of Ag NPs and antireflection of SiO_2 ARC. Practically, the back-scattering of Ag NPs was reduced and re-coupled it into the active layer for the cells with Ag NPs embedded in SiO_2 ARC.

4 Conclusions

The obtained results of Raman and absorbance examined the plasmonic effects of Ag NPs embedded and non-embedded in SiO_2 with various dimensions and revealed that the large dimensions of Ag NPs exhibited much impressive plasmonic effects. Moreover, optical reflectance and photovoltaic current–voltage measurements were also used to confirm the photovoltaic performance enhancement inducing by plasmonic effects of Ag NPs. For Ag NPs on the thin SiO_2 space layer (non-embedded), the efficiency enhancement of 8.77% (from 11.97 to 13.02%) of the cell with Ag NPs of 32-nm dimension was obtained, compared to the cell with a thin SiO_2 space layer. Furthermore, the efficiency enhancement of 10.24% (from 13.47 to 14.85%) of the cell with Ag NPs of 32-nm dimension embedded in SiO_2 ARC was obtained. The gain of 1.38% in absolute efficiency of the cell with Ag NPs of 32-nm dimension embedded in SiO_2 ARC was obtained and the gain indicated the potential benefit of Ag NPs embedded in SiO_2 ARC due to additional plasmonic effects on the cell, compared to the cell with a pure SiO_2 ARC.

Acknowledgements The authors would like to thank the Ministry of Science and Technology of the Republic of China for financial support under Grant MOST 103-2221-E-027-049-MY3.

References

1. S.A. Maier, H.A. Atwater, Plasmonics: localization and guiding of electromagnetic energy in metal/dielectric structures. *J. Appl. Phys.* 98, 011101–1–011101-10 (2005)
2. J.A. Schuller, E.S. Barnard, W. Cai, Y.C. Jun, J.S. White, M.L. Brongersma, Plasmonics for extreme light concentration and manipulation. *Nat. Mater.* 9, 193–204 (2010)
3. N. Olivia, P. Francisco, R.K. Leary, D.J. Holland, C. Ducati, P.A. Midgley, Three-dimensional imaging of localized surface plasmon resonances of metal nanoparticles. *Nature* 502, 80–84 (2013)
4. X.C. Ma, Y. Dai, L. Yu, B.B. Huang, Energy transfer in plasmonic photocatalytic composites. *Light* 5, e16017 (2016)
5. C.L. Tan, S.J. Jang, Y.T. Lee, Localized surface plasmon resonance with broadband ultralow reflectivity from metal nanoparticles on glass and silicon subwavelength structures. *Opt. Express* 20(16), 17448–17455 (2012)
6. H.A. Atwater, A. Polman, Plasmonics for improved photovoltaic devices. *Nat. Mater.* 9, 205–213 (2010)
7. K.A. Willets, R.P.V. Duyne, Localized surface plasmon resonance spectroscopy and sensing. *Annu. Rev. Phys. Chem.* 58, 267–297 (2007)
8. L. Manai, B.D. Rezgui, R.B. Zaghouni, D. Barakel, P. Torchio, O. Palais, B. Bessais, Tuning of light trapping and surface plasmon resonance in silver nanoparticles/c-Si structures for solar cells. *Plasmonics* 11, 1273–1277 (2016)
9. Y.W. Ma, Y. Zhang, Z.W. Wu, L.H. Zhang, J. Zhang, G.S. Jian, S.F. Wu, Theoretical studies of the optical properties of plasmon resonance on silver nanoparticles in the near-field optics. *J. Appl. Phys.* 105, 103101-1–103101-6 (2009).
10. M.S. Golden, A.C. Bjonnes, R.M. Georgiadis, Distance- and wavelength-dependent dielectric function of Au nanoparticles by angle-resolved surface plasmon resonance imaging. *J. Phys. Chem. C* 114, 8837–8843 (2010)
11. C. Noguez, Surface plasmons on metal nanoparticles: The influence of shape and physical environment. *J. Phys. Chem. C* 111, 3806–3819 (2007)
12. T. Sandu, Shape effects on localized surface plasmon resonances in metallic nanoparticles. *J. Nanopart. Res.* 14(905), 1–10 (2012)
13. V. Amendola, O.M. Bakr, F. Stellacci, A study of the surface plasmon resonance of silver nanoparticles by the discrete dipole approximation method: effect of shape, size, structure, and assembly. *Plasmonics* 5, 85–97 (2010)
14. J.J. Mock, D.R. Smith, S. Schultz, Local refractive index dependence of plasmon resonance spectra from individual nanoparticles. *Nano Lett.* 3(4), 485–491 (2003)
15. Z.A. Garmaroudi, M.R. Mohammadi, Plasmonic effects of infiltrated silver nanoparticles inside TiO₂ film: enhanced photovoltaic performance in DSSCs. *J. Am. Ceram. Soc.* 99(1), 167–173 (2016)
16. A.J. Haes, R.P.V. Duyne, A unified view of propagating and localized surface plasmon resonance biosensors. *Anal Bioanal Chem* 379, 920–930 (2004)
17. V. Mankad, R.K. Kumar, P.K. Jha, Investigation of blue-shifted plasmon resonance: an optical properties study of silver nanoparticles. *Nanosci. Nanotechnol. Lett* 5, 1–6 (2013)
18. J.L. Wu, F.C. Chen, Y.S. Hsiao, F.C. Chien, P. Chen, C.H. Kuo, M.H. Huang, C.S. Hsu, Surface plasmonic effects of metallic nanoparticles on the performance of polymer bulk heterojunction solar cells. *ACS Nano* 5(2), 959–967 (2011)
19. P. Mandal, S. Sharma, Progress in plasmonic solar cell efficiency improvement: a status review. *Renew. Sustain. Energy Rev.* 65, 537–552 (2016)
20. S. Pillai, K.R. Catchpole, T. Trupke, M. A. Green, Surface plasmon enhanced silicon solar cells. *J. Appl. Phys.* 101, 093105-1–093105-8 (2007).
21. S.K. Sardana, S.N.C. Venkata, E. Thouti, N. Chander, S. Kumar, S.R. Reddy, V.K. Komarala, Influence of surface plasmon resonances of silver nanoparticles on optical and electrical properties of textured silicon solar cell. *Appl. Phys. Lett.* 104, 073903 (1–5) (2014)
22. M. Notarianni, K. Vernon, C.A. Alison, M. Aljada, J. Liu, N. Motta, Plasmonic effect of gold nanoparticles in organic solar cells. *Sol. Energy* 106, 23–37 (2014)
23. J.W. Leem, S. Kim, C. Park, E. Kim, J.S. Yu, Strong photocurrent enhancements in plasmonic organic photovoltaics by biomimetic nanoarchitectures with efficient light harvesting. *ACS Appl. Mater. Interfaces* 7(12), 6706–6715 (2015)
24. M.A.K.L. Dissanayake, J.M.K.W. Kumari, G.K.R. Senadeera, C.A.Thotawatthage, Efficiency enhancement in plasmonic dye-sensitized solar cells with TiO₂ photoanodes incorporating gold and silver nanoparticles. *J Appl Electrochem* 46, 47–58 (2016)
25. C. Pahud, O. Isabella, A. Naqavi, F. Haug, M. Zeman, H.P. Herzig, C. Ballif, Plasmonic silicon solar cells: impact of material quality and geometry. *Opt. Express* 21(S5), A786–A797 (2013)
26. Q. Xu, C. Johnson, C. Disney, S. Pillai, Enhanced broadband light trapping in c-Si solar cells using nanosphere-embedded metallic grating structure. *IEEE J. Photovolt* 6(1), 61–67 (2016)
27. W.J. Ho, S.Y. Su, Y.Y. Le, H.J. Syu, C.F. Lin, Performance-enhanced textured silicon solar cells based on plasmonic light scattering using silver and indium nanoparticles. *Materials* 8(10), 6668–6676 (2015)
28. W.J. Ho, Y.Y. Lee, C.H. Lin, C.W. Yeh, Performance enhancement of plasmonics silicon solar cells using Al₂O₃/In NPs/TiO₂ antireflective surface coating. *Appl. Surf. Sci.* 354, 100–105 (2015)
29. A.R. Bijanzadeh, M.R. Vakili, R. Khordad, A study of the surface plasmon absorption band for nanoparticles. *Int. J. Phys. Sci.* 7(12), 1943–1948 (2012)
30. Y. Flegler, M. Rosenbluh, Surface plasmons and surface enhanced Raman spectra of aggregated and alloyed gold-silver nanoparticles. *Int. J. Optics* 2009, 1–5 (2009)
31. C.-B. Wang, G. Deo, I.E. Wachs, Interaction of polycrystalline silver with oxygen, water, carbon dioxide, ethylene, and methanol: in situ Raman and catalytic studies. *J. Phys. Chem. B* 103, 5645–5656 (1999)
32. A.K. Yadav, P. Singh, A review of the structures of oxide glasses by Raman spectroscopy. *RSC Adv* 5, 67583–67609 (2015)